 doi:10.20944/preprints202110.0283.v1

Article

Innovative energy-saving propulsion system for low-speed biomimetic underwater vehicles

Paweł Piskur [1,‡*], Piotr Szymak [1,‡], Michał Przybylski [1,‡], Krzysztof Naus [2,‡], Krzysztof Jaskólski [2,‡], Mariusz Żokowski [3,‡],

[1] Polish Naval Academy; Faculty of Mechanical and Electrical Engineering; Smidowicza 69; Gdynia; Poland
[2] Polish Naval Academy; Department of Navigation; Smidowicza 69; Gdynia; Poland
[3] Air Force Institute of Technology; ks. Boleslawa 6; Warsaw; Poland
* Correspondence: p.piskur@amw.gdynia.pl
‡ These authors contributed equally to this work.

Abstract: This article covers research on an innovative propulsion system design for a Biomimetic Unmanned Underwater Vehicle (BUUV) operating at low speeds. The experiment was conducted on a laboratory test water tunnel equipped with specialised sensor equipment to assess the Fluid-Structure Interaction (FSI) and energy consumption of two different types of propulsion systems. The experimental data contrasts the undulating with the drag-based propulsion system. The additional joint in the drag-based propulsion system is intended to increase thrust, decrease energy input, and protect the fins from degradation due to fatigue. The tests were conducted at a variety of fins oscillation frequencies and fluid velocities. Experiments demonstrate that in the region of low-speed forward movement, the efficiency of the propulsion system with the additional joint is greater.

Keywords: Biomimetic Unmanned Underwater Vehicle (BUUV); fish-like movement; underwater robotics; energy efficiency; Fluid-Structure Interaction (FSI); undulating propulsion

1. Introduction

Biomimetic propulsion systems are based on biological organisms that evolved through natural selection over many years [1]. In contrast to the screw-type propeller system, the biomimetic ones move like a fish [2], a turtle [3], or a seal [4]. The undulatory movement of body bending generates propulsion by pushing the water against the passing wave [5]. Because of the benefits of a low hydroacoustic noise spectrum [6], this type of propulsion is becoming more popular in underwater robots [7], [8]. However, the influence of tail oscillation on the fluid flow around a hull causes vortices and the need to carefully study the FSI [9], [10] and the vortex structures [11]. Underwater vehicles shown in publication [12], [7] have propulsion systems made of several moving parts. For example, the artificial fish in Fig. 1a is shown with a hull formed by the coupling of rigid movable parts with a flexible fin [13] at the end. This type of construction is difficult to control, expensive and increases the risk of flooding electronic components inside. That is why an effort was made to design a biomimetic propulsion system based on single, flexible fins [14]. The BUUV with a propulsion system consisting of one flexible tail fin and two side fins is depicted in Fig. 1b. This kind of propulsion made it challenging to maintain the BUUV's direction. Furthermore, if hydroacoustic sensors are to be employed, movement stabilisation is highly desirable. To increase course stability and reduce scrolling impact, [4] replaced one tail fin with two tail fins (Fig. 1c).

A proposed innovative propulsion system is a modified version of two-tail fins propulsion system [4] with reduced drag during the return stroke thanks to the use of an additional joint. The propulsion

Preprints (www.preprints.org) | NOT PEER-REVIEWED | Posted: 20 October 2021 doi:10.20944/preprints202110.0283.v1

(a) (b) (c)

Figure 1. BUUV with propulsion system made of: (a) movable, rigid elements and flexible fin [6]; (b) one flexible tail fin [15]; (c) two flexible tail fins [16].

design with the additional joint is distinct from prior designs [17], [18], [19], [20] particularly during the return movement. Under the effect of fluid drag force, the fin is freely rotated up to 90 degrees during the return stroke.

Although, the authors' paper [21] offered a simulation analysis of a fin drag force in a BUUV using the LS-DYNA software and Incompressible Computational Fluid Dynamics (IFCD) with validation in a water tunnel, in this paper data are provided based on the measurements made in the water tunnel. This is mainly due to the fact that the thrust and the drag of fins depend on their flexibility and shape for different fluid velocities as well as different frequencies and different amplitudes of oscillation.

The only one piece of the fish-like flapping foils and one flipper with an additional join were compared because they can be used on both sides of the vehicle (pectoral fins) as well as at the aft of the BUUV (caudal fins). The fin system in tandem is to be compared in a later study, and in that case, the paper concentrates on the mechanism's dynamic of the propulsion system based on one fin.

The efficiency comparison between two types of propulsion system is provided according to the research and the analysis presented in papers [22], [23], [24], where defined efficiencies take under consideration the kinematic and performance parameters for various measurement conditions.

The following section depicts a description of the new propulsion system with the additional joint. The laboratory test equipment, measurement method, and test provided are then discussed. The new propulsion system's mathematical analysis is then provided with a discussion on energy efficiency. Finally, the following section compares the results of measurements for the new propulsion system with additional joint to the fish-like flapping foils one. At the end of this study, the findings are discussed, and conclusions and future research directions are proposed.

2. Description of the new propulsion system with additional joint

The photo sequence is shown in Fig. 2 to help describe the new drive mechanism. The two fins mounted on its stern to the vertical rotary axes are tilted synchronously in a horizontal plane by electric motors to ensure the underwater vehicle's translational movement. In power stroke, the BUUV moves the stern fins from outside to the back to push the water in opposite direction to the hull movement (Fig. 2 b-c-d). In return stroke, the BUUV moves the stern fins to start position with the drag force reduction provided by the additional joint (Fig. 2 e-f-g). The movement of both fins outwards is just an auxiliary movement that allows the specified values of the maximum angular deflection of the fins regarding the longitudinal axis of symmetry to be obtained, which is required to begin the work movement. During the movement fins' alter their position from the vertical to the horizontal plane. It reduces the hydrodynamic drag of the fins during outside movement and, as a result, the drag of underwater vehicles.

The main benefit of the auxiliary joint is a seamless quarter turn to a position with the least amount of drag. The next benefit of the proposed concept is that the auxiliary joint does not require a separate servo motor [17].

The second portion of the paper provides a more extensive analysis that excludes the impact of the hull on the propulsion system parameters.

Preprints (www.preprints.org) | NOT PEER-REVIEWED | Posted: 20 October 2021 doi:10.20944/preprints202110.0283.v1

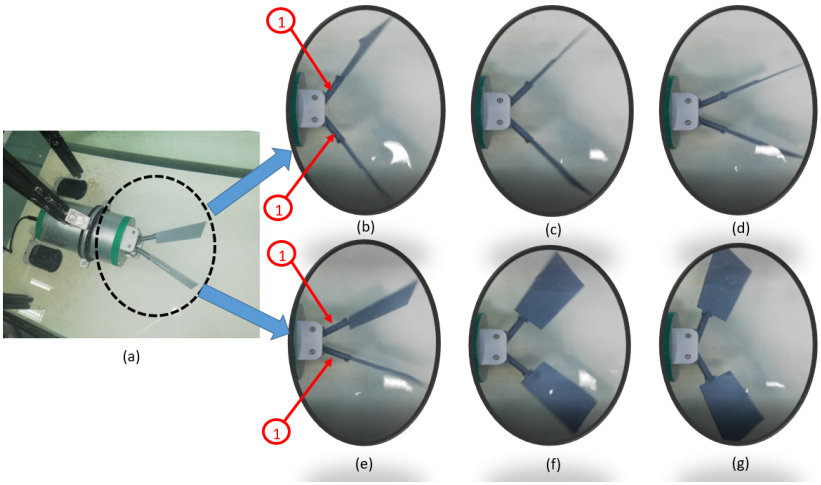

Figure 2. The BUUV (a) with subsequent phases of movement: (b), (c), (d) power stroke, (e), (f), (g) return stroke; 1 - additional joints

2.1. Fins used for testing

In the paper [25], a wide range of real caudal fin shape species were digitised and analysed, ranging from homocercal tails with a low aspect ratio (square shape used by bluegill sunfish and rainbow trout) to high aspect ratio (lunate shape adopted by tuna and swordfish), and even heterocercal caudal fin adopted by sharks. The comparison of propulsive efficiency shows that large aspect ratio fins (tuna and shark) are more efficient while cruising ($St < 0.4$), whereas short aspect ratio caudal fins (catfish and trout) are more efficient when fish are accelerating or manoeuvring ($St > 0.4$). Given that vortex morphologies are primarily reliant on the fin aspect ratio and trailing edge shape [26], the rectangular shape of the fins was chosen for the study and comparing the efficiency changes caused by the addition of a joint.

In Fig. 3, two fins with the same length (70 mm) and height (40 mm) are displayed. The variable M indicates the torque from the servomechanism while the variable u indicates the BUUV velocity relative to the water. The fish-like flapping foils (Fig. 3 a, b) made from flexible, thin steel sheet and flexible polycarbonate were chosen according to earlier experimental testing [27]. The flexibility parameter was selected by changing the thickness of the fin. Due to the needed flexibility and fatigue strength [28], the polycarbonate fin has a width of 0.2 mm , whereas the steel fin has a width of 0.1 mm.

In Fig. 3 c, d the fin with the additional joint is presented for power (c) and return (d) stroke. The vertical position of the inflexible fin with additional joint (Fig. 3 c) generates thrust, while the horizontal position (Fig. 3 d) is used to reduce resistance on the return stroke.

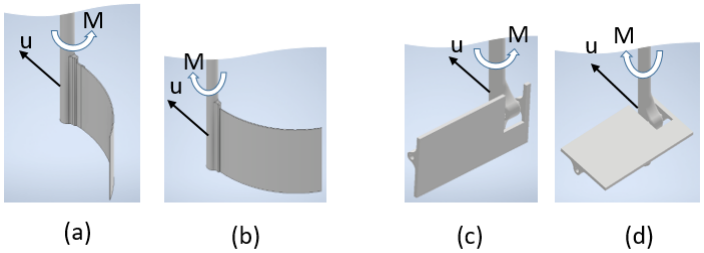

Figure 3. Two types of propulsion systems used for tests: the flexible fin during counterclockwise (a) and clockwise (b) movement; the flipper with additional joint during power (c) and return (d) stroke

Preprints (www.preprints.org) | NOT PEER-REVIEWED | Posted: 20 October 2021 doi:10.20944/preprints202110.0283.v1

2.2. Laboratory test equipment and measurements method

The laboratory test water ring shown in Fig. 4 was designed for the characteristic dynamic establishment of the singular fin without considering the effect of the underwater vehicle body. The laboratory water tunnel was composed of polyethylene panels with the following dimensions: 0.09 m height, 0.22 m width, and 0.02 m^2 cross-sectional area. The laboratory test determines the fin dimensions to stand as well as the sensors employed. For example, too large fin may interact with the inner sides of the tunnel, while too tiny a fin may generate insufficient force to be monitored by strain gauges. Corners were set to 45° due to laminar flow restrictions, and an additional steering wheel was installed before the place of measurement. An external water pump with adjustable fluid velocity was used to provide experiments with varying fluid velocities. Using signals from the high-precision, non-invasive ultrasonic flow meter the water velocity was managed in a closed-loop control system [29]. Two strain gauges were positioned symmetrically on both sides of the water tunnel to assess the fluid-structure interaction. Both strain gauges were attached to the ground on one side and to the transparent plate (made of polycarbon) on the other. Ball bearings support a polycarbonate plate to prevent friction. A servomechanism (Dynamixel MX-12W) is installed in the centre of the polycarbonate plate for fin movement. The significant characteristics of the Dynamixel MX-12W are stall torque (M) of 0.2 Nm (at 12 V, 1.4 A) and a top speed of 470 rpm (revolutions per minute). This allows fins to be moved with oscillation motions of up to 7.8 Hz for unload movement. The force between the fin and the water was measured directly using different fins linked to the servomechanism. Furthermore, the control algorithm was used for water velocity and fin frequency, and amplitude with restrictions on the desired Strouhal number. Finally, the trailing edge's peak-to-peak amplitude was measured using the vision algorithm described in the authors' paper [30].

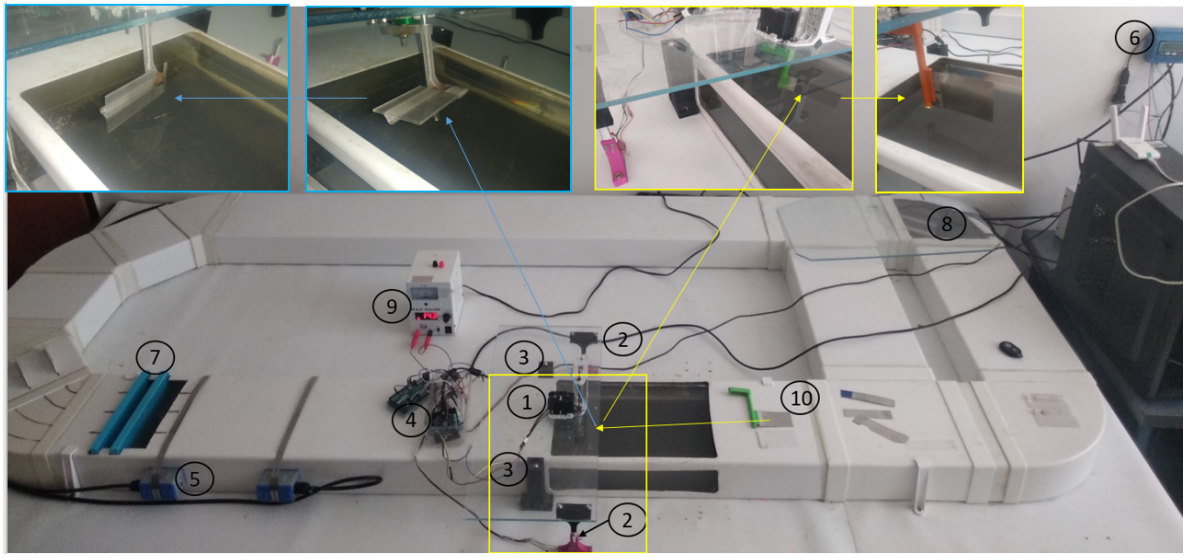

Figure 4. The laboratory water tunnel: 1 – servomechanism Dynamixel MX-12W, 2 – strain gauges, 3 - ball bearings, 4 - micro-controller unit (MCU) and strain gauges amplifier, 5 – ultrasonic flow sensors, 6 - ultrasonic flow unit, 7 – water steering wheels, 8 – external water pump, 9 – power supply, 10 - the fin

3. Mathematical relations

The analysis was carried out following the Buckingham theory [31]. The principle enables the expression of all the information contained in the problem's interactions between physical variables in a very compact manner, employing a reduced number of dimensionless variables. According

Preprints (www.preprints.org) | NOT PEER-REVIEWED | Posted: 20 October 2021 doi:10.20944/preprints202110.0283.v1

to a review of the literature [32], [33] and experimental results, the expression characterising the fluid-structure interaction can be described as follows:

$$F = f(K, \alpha, St, Re, k) \tag{1}$$

where:
K - a geometric parameter that determines the shape of the fin;
α - the angle of attack, measured between the fin chord and the fluid velocity;
St - Strouhal [34] number depicted in equation (2) ;
Re - Reynolds [35] number, here defined as a ratio of fluid inertia to viscous forces (equation 3);
k - a stiffness coefficient [36] (equation 4);

$$St = f\frac{A}{u_\infty} \tag{2}$$

$$Re = \frac{cu_\infty}{\mu} \tag{3}$$

$$k = \frac{EI}{\rho u_\infty^2 c^3} \tag{4}$$

where:
f - the fin movement frequency;
A - a peak-to-peak amplitude measured at the fin trailing edge;
u_∞ - a free stream fluid velocity;
c - the chord length of the fin at the midline;
μ - a fluid viscosity;
E - Young's modulus;
$I = \frac{h^3}{12}$ - the area moment of inertia of the cross section;
ρ - a fluid density.

3.1. *Fluid-structure-interaction force for innovative propulsion system as a function of two angles*

According to equation (5), the force during the working and returning movement of a fin depends on the coefficient (C_f), the side area of the fin (S), both angles α and β, the square of the fluid velocity (u) and acceleration concerning the fin as well as an added mass (m).

$$F(\alpha, \beta) = m(\alpha, \beta)\frac{du}{dt} + \frac{1}{2}\rho S(\alpha, \beta)C_f(\alpha, \beta)u^2 \tag{5}$$

where:
α - an angle of attack in the horizontal plane;
β - an angle of attack in the vertical plane;
m - is an added mass;
$C_f(\alpha, \beta)$ - is measured experimentally in the laboratory water tunnel [21], [29].

The force (F) is affected by the position of the fin and the velocity of the water. For $\alpha = 90^\circ$ and $\beta = 0^\circ$, the fin is in a neutral position parallel to the vehicle's longitudinal axis, whereas $\alpha = 0^\circ$ and $\beta = 90^\circ$ indicate that the fin is entirely deflected in an outwards position.

The reaction force generated by this impulsive motion in water can generate considerable thrust proportional to the fin acceleration. The actual force can be difficult to assess accurately because it is difficult to estimate precisely the volume of fluid that is accelerated by a particular motion. Although for simple motions and shapes, some reasonable estimates can be given, here experiments in the water tunnel were provided.

Preprints (www.preprints.org) | NOT PEER-REVIEWED | Posted: 20 October 2021 doi:10.20944/preprints202110.0283.v1

3.2. Efficiency of the propulsion system

The energy efficiency of the propulsion system [22], [37] is defined as the ratio of useful power output to the rate of power input measured over a specific time interval [38], [39].

$$\eta = \frac{uT_n}{P_f} \tag{6}$$

where:
η - the energy efficiency;
T_n - the net thrust;
u - a water speed;
P_f - a value of electrical power consumed by the servomotor.

For very low Reynolds number viscous forces produce both the drag and the thrust forces. Also, propulsion forces generated by fin deformation or flipper position and velocity influence the drag forces, for that reason presented in equation (6) the net thrust defines the difference between thrust and drag force (7).

$$T_n = T + T_D \tag{7}$$

where:
T - the thrust;
T_D - the drag force.
For a propulsion system submerged in a viscous fluid, the propulsor thrust needs to overcome the resistance force for ensuring a constant speed. A steady motion for $T_n = 0$ means that the propulsion system does not decelerate or produce thrust.

Power input to the servomotor [40] is determined as a product of the measured voltages (U) and the electric current (I) [41] across the servomotor using the following equation (8):

$$P = IU \tag{8}$$

In Fig. 5 the two P_s and P_f are the power consumed by the servomotor when driving without the fin and when driving the fin in water, respectively. The data reported here were achieved by experimentation on the tested fin. The tests were provided for the frequency of the fin oscillation in the range from 1 to 7.6 Hz.

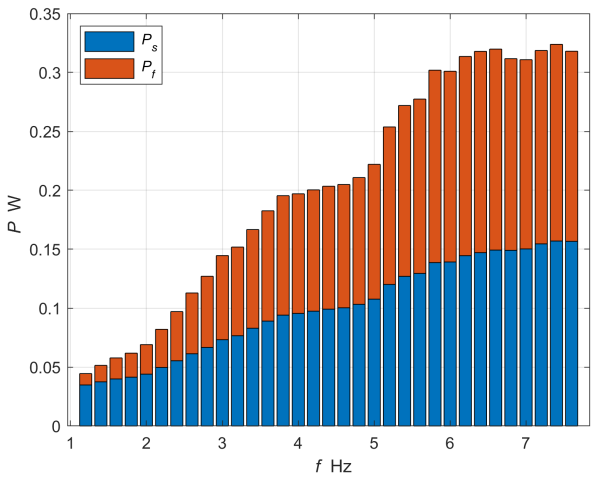

Figure 5. Electric power delivered to the servomotor: P_s - power for servomotor without fin, P_f - power for fin submerged in the water

Preprints (www.preprints.org) | NOT PEER-REVIEWED | Posted: 20 October 2021 doi:10.20944/preprints202110.0283.v1

4. Results and discussion

For the proposed propulsion system, the example of the net thrust measurement result as a function of time with oscillation frequency $f = 0.7\ Hz$ is presented in Fig. 6. On the left side of the figure the position of the fin is presented during the power stroke (upper part) and during the recovery stroke (lower part). As it can be seen in Fig. 6, the measured value of FSI is characterized by fluctuations of the function of time. Therefore, the final values of the net thrust and frequency presented in the further part of the paper were received by averaging over ten periods of servomotor oscillations.

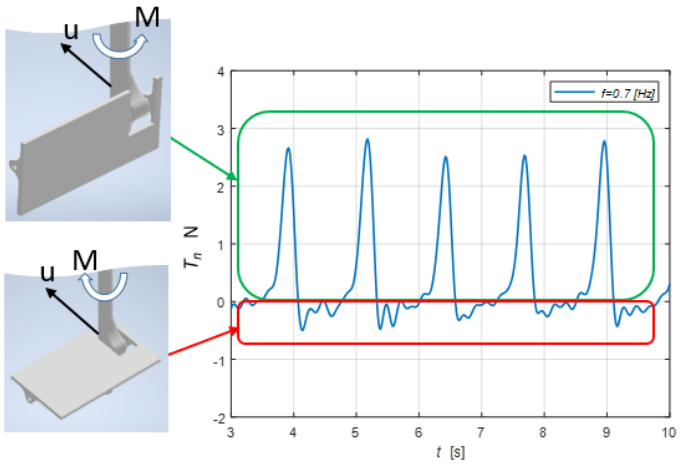

Figure 6. The net thrust as a function of time for undulating frequency $f = 0.7\ Hz$

Both kinds of propulsion systems were tested for different frequencies of the fins oscillation and for different water velocities as well. The same frequency was used for each tested fin to limit the number of dependent variables. The mean value of the difference between the thrust and the drag force (the net thrust) was measured according to formula (7) and presented in (Fig. 7 - 13).

Fig. 7 - 9 show a series of mean values of the net thrust as a function of fin movement frequency for different water velocity. An external water pump was used to control the water velocity in the water tunnel to imitate FSI, like for the fin's forward speed in relation to the water. The water velocity varied between zero and twenty centimeters per second (u = 0.2 m/s). The mean thrust for all frequencies was most significant when the water velocity was equal to zero (u = 0 m/s). For that measurement condition, the drag force was equal to zero for fish-like flapping foils. While for the fin with additional joint, the thrust was much higher than the drag force. The mean net thrust for flexible polycarbonate fin movements at a frequency of 1 Hz was up to 40 mN. Increasing the frequency up to 4 Hz, the net thrust increased up to 140 mN (Fig. 7). Raising the frequency further does not increase the mean net thrust. Increasing the fluid's speed simulates the fin's movement against the fluid. When the velocity of the water increases, the tested fins must overcome fluid resistance. As a result, as the water velocity increases, the average net thrust decreases. The nature of the changes in the mean net thrust is revealed by the approximation of the set of measurement points. It can also be seen that for flexible fins (placed along the fluid stream) at low frequencies, the mean net thrust rapidly increases with increasing fin frequency, reaches a maximum, and then remains constant with further increases in fin frequency oscillation movement (Fig. 7 - 8). For fin with additional axis of rotation, the mean thrust increases with respect to the fin oscillation frequency (Fig. 9) according to the equation (5). This is because a higher fin oscillation frequency creates a faster fin velocity through the fluid. Hence the driving force increases by the square of the speed. Also, during the return movement, the drag force is proportional to the speed, but the drag coefficient (C_f) and frontal surface ($S(\alpha, \beta)$) decrease due to the rotation of the fin to 90° provided by the additional joint. Furthermore, the acceleration can be adjusted so that according to equation (5) the forward acceleration can be greater than the return acceleration.

Preprints (www.preprints.org) | NOT PEER-REVIEWED | Posted: 20 October 2021 doi:10.20944/preprints202110.0283.v1

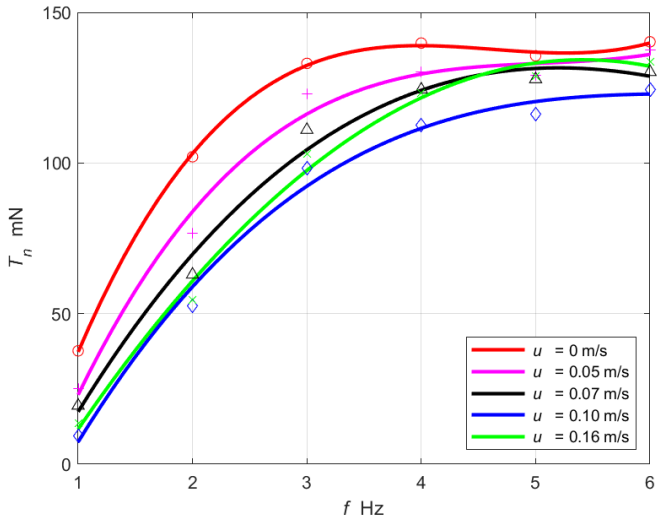

Figure 7. A mean value of the net thrust for flexible fin made from polycarbonate

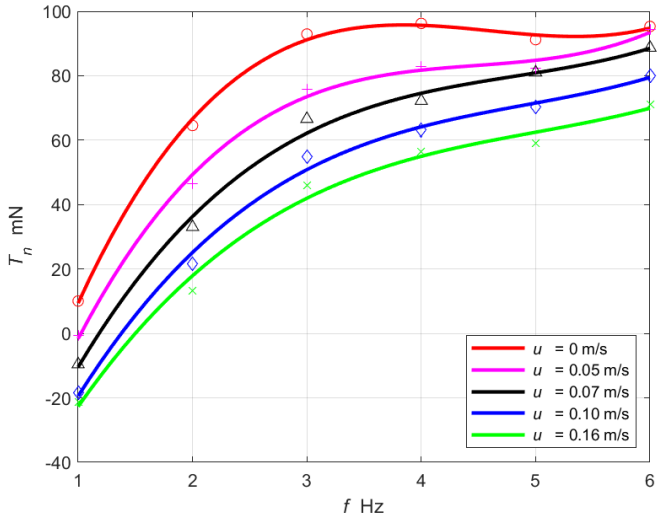

Figure 8. A mean value of the net thrust for a flexible fin made from thin steel sheet

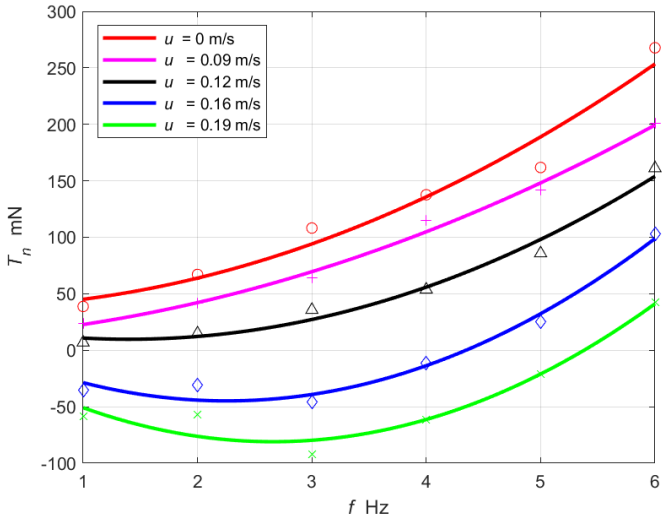

Figure 9. A mean value of the net thrust for inflexible fin with additional joint

Preprints (www.preprints.org) | NOT PEER-REVIEWED | Posted: 20 October 2021 doi:10.20944/preprints202110.0283.v1

Fig. 10 shows the relationship between the net propulsive efficiency as a function of the Strouhal number. For varied fin frequencies, trailing edge amplitude, and fluid velocity, the same Strouhal number can be obtained. According to the equation (2), as the frequency of the fin movement rises and the water speed increases, the Strouhal number may remain constant, but the net propulsive efficiency varies. Taking under consideration the nature of the characteristic changes, it can be seen that the net propulsive efficiency increase due to the Stouhal number for the propulsion system with the additional joint. Fig. 10 shows that flexible fins have a form comparable to the conventional efficiency curve displaying efficiency as a function of Strouhal number given in works [24] and [42]. The observed results are compatible with the literature research [43], [44] which has revealed that the optimal efficiency [45] of the drive system for fish-like movements improves in the Strouhal number range of 0.25 to 0.35 [34]. Further, the stiffness [46] difference between the tested fish like flapping foils (polycarbonate and steel fins) is responsible for the differences. During the investigation, there were more different varieties of polycarbonate fins. Thus, the best one was chosen from a wide range of flexible parameters. There were not as many flexible fins available among thin sheet steel fins.

The net efficiency is zero when the mean net thrust is zero, which means that the thrust compensates for the drag force.

If the thrust is lower than drag force, then the net efficiency is negative. It means that the fluid velocity in the water tunnel is higher than the propulsion system would move forward in an unmovable fluid.

If the resistance of the investigated propulsion system were known, then the quasi-propulsive efficiency defined in the paper [22] could be calculated. This could provide a more intuitive description of the efficiency with including the resistance. Then, there would not be a negative value of efficiency. For the propulsion system tested, the distinction between thrust and drag force cannot be made. The negative efficiency means that, at constant water speed, the propulsion system cannot compensate for the drag such as to keep the cruising velocity (u).

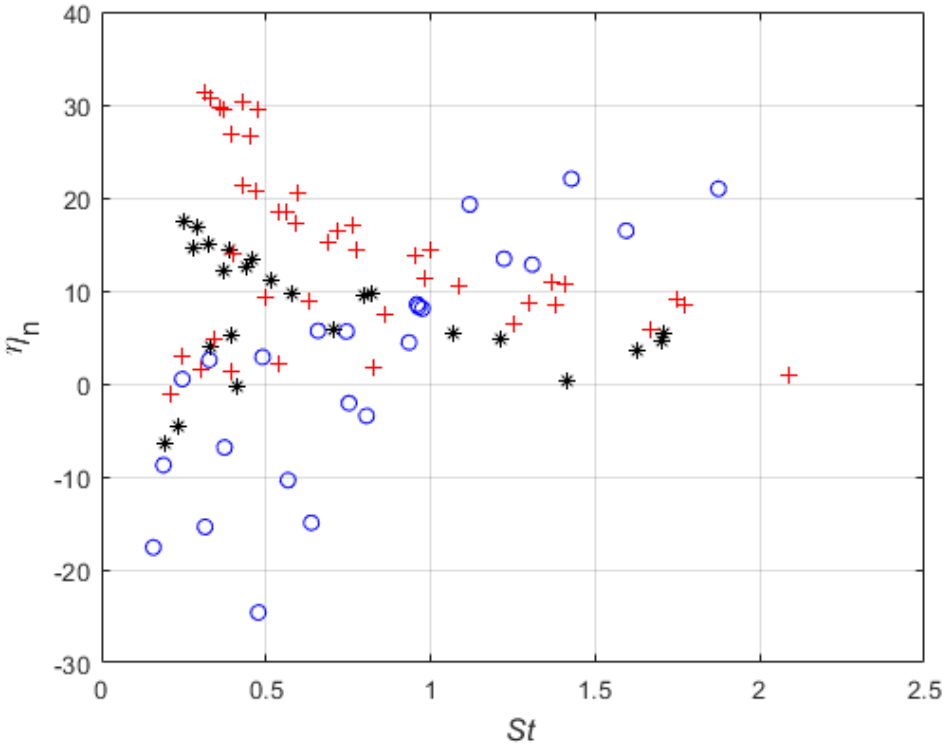

Figure 10. The net propulsive efficiency as a function of Strouhal number for fin:
+ made from polycarbonate , o with additional joint, ∗ made from thin steel sheet

Preprints (www.preprints.org) | NOT PEER-REVIEWED | Posted: 20 October 2021 doi:10.20944/preprints202110.0283.v1

The design of the propulsion system, with an additional joint, achieves the best net efficiency for Strouhal numbers more significant than 1, indicating that the water velocity is equal to zero (Fig. 11) or has a low value (Fig. 12). This is analogous to fish that use a pectoral fin to swim at a slow speed but with high-energy efficiency [47].

In addition, it can be shown in Fig. 11 - 13 that the net thrust for propulsion system with additional joint, increases with higher frequency, according to the mathematical relationship in equation (5).

For the results presented in Fig. 11, where the water velocity is equal to zero, the thrust was measured for the drag force equal to zero. It means that for that measurement condition, only the thrust is generated. It can be seen from the experimental measurements, that the fin with additional joint has almost two times higher thrust that the fish like flapping foils propulsion system.

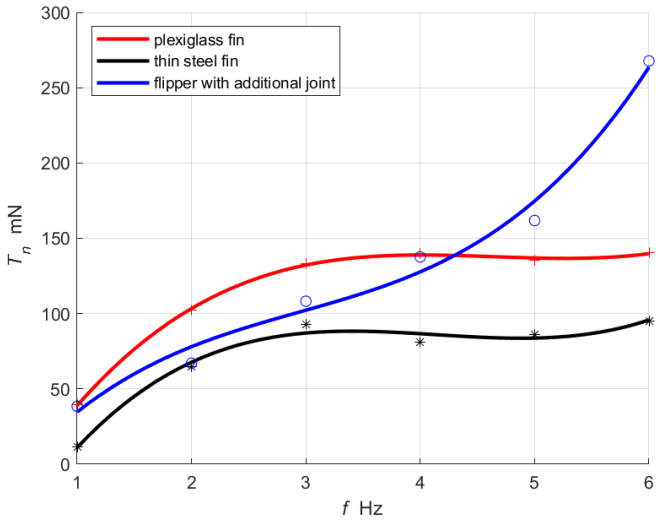

Figure 11. The mean thrust generated by fins for different frequency, and fluid velocity $u = 0\ m/s$

Fig. 12 indicates the mean value of the net thrust higher for the propulsion system with the additional joint in comparison to fish-like flapping foils. Furthermore, the proportional relationship between thrust and fin frequency strengthens the BUUV's course control. When hydroacoustic sensors are utilised [48], this control condition is desirable for the BUV [49]. The measurements with propulsion system implemented as a pectoral and/or caudal fin is to be the subject of the next research.

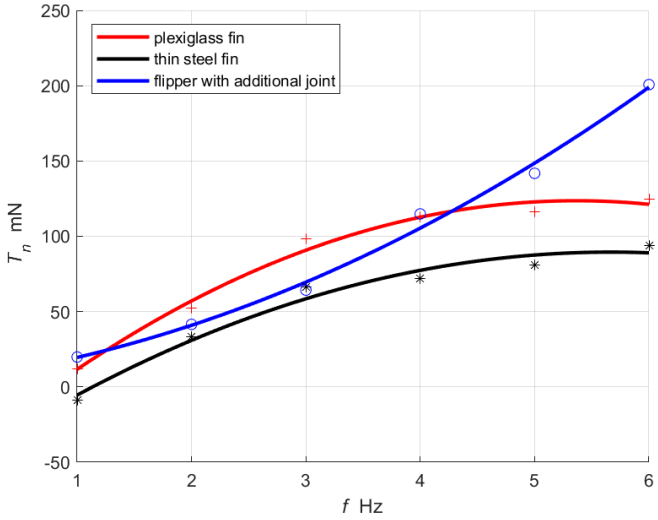

Figure 12. The mean net thrust generated by fins for different frequency, and fluid velocity $u = 0.1\ m/s$

Preprints (www.preprints.org) | NOT PEER-REVIEWED | Posted: 20 October 2021 doi:10.20944/preprints202110.0283.v1

For the highest value of water velocity available in the water tunnel (Fig. 13) the propulsion system with additional joint has a lower value of the net thrust than both fish-like flapping foils propulsion systems. Also, it is worth noticing that for water velocity $u = 0.2\ m/s$, the net thrust force characteristics crosses the zero for all the tested fins. This gives information about the frequency needed to generate thrust to overcome the drag force and to swim with a constant speed. This also leads to further research on the propulsion system, which will cover the combination of flexible fins with an additional joint.

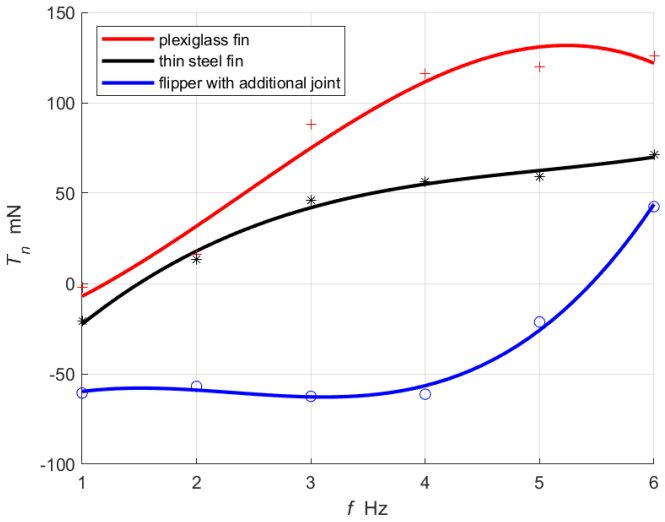

Figure 13. The mean net thrust generated by fins for different frequency, and fluid velocity $u = 0.2\ m/s$

5. Conclusion and future work

In the domains of bio-locomotion and biomimetics, the study of bodies moving in a fluid is an intriguing and challenging research topic. The number of design and control variables was decreased to demonstrate the difference between an innovative propulsion system and the undulating one. Increasing the velocity of the fins during thrust generation while decreasing the velocity of the fins during the returning movement should result in even better efficiency. The fin velocity herein was determined by the specifications of the available servomotors and water tunnel dimensions. The proposed propulsion system design has higher thrust and the higher net efficiency for low-speed movement ensures the biomimetic nature of the movement.

The future tests are going to be provided with including body impact on the propulsion system characteristics. The findings encourage further investigation into the effects of mass ratio, non-uniform stiffness, and background turbulence on the unsteady dynamics.

The future research will concentrate on the Particle Image Velocimetry (PIV) approach, which will be used to conduct a more in-depth investigation of the Fluid-Structure Interaction (FSI). This analysis method allows comparing the created thrust to the speed of the water near the fins. The test will be provided to build a propulsion system with additional joint and flexible fins and various movement styles. This can lead to a more accurate replica of the living marine organism with high-energy efficiency. Finally, the promising results presented in the paper enable us to expect to obtain more efficient undulating propulsion for the BUUV in the close future.

6. Patents

On 2019-12-06, the propulsion system design named: "Multi-fin wave thruster with resistance reduction in the return cycle, especially for a biomimetic underwater vehicle" was registered at the

Patent Office of the Republic of Poland under the number P.432101. The patent application process is now underway.

Author Contributions: Conceptualization, P.Sz. and P.P.; methodology, P.Sz. and P.P.; software, P.Sz. and P.P.; validation, P.P.; formal analysis, P.P.; investigation, P.Sz., P.P., M.P. ; resources, P.Sz., P.P., M.Ż.; data curation, P.Sz., P.P.; writing-original draft preparation, P.P.; writing-review and editing, P.Sz., K.N., K.J., M.Ż.; visualization, P.P., P.Sz..; supervision, P.Sz., K.N., K.J.; project administration, P.P.; funding acquisition, P.Sz.

Funding: The paper is financed by a Polish Ministry of Defense Research Grant titled "Model studies of the characteristics of an undulating propulsion system."

Conflicts of Interest: The authors declare no conflict of interest.

Abbreviations

The following abbreviations are used in this manuscript:

AR - Aspect Ratio;
BL/s - Body Length per second;
BUUV - Biomimetic Unmanned Underwater Vehicle;
PIV - Particle Image Velocimetry;
RPM - Revolutions Per Minute;
MCU - micro-controller unit;
FSI - Fluid Structure Interaction.

References

1. Mannam, N.P.B.; Krishnankutty, P. Biological Propulsion Systems for Ships and Underwater Vehicles. In *Propulsion Systems*; IntechOpen, 2019; p. 113. doi:10.5772/intechopen.82830.
2. Sitorus, P.E.; Nazaruddin, Y.Y.; Leksono, E.; Budiyono, A. Design and Implementation of Paired Pectoral Fins Locomotion of Labriform Fish Applied to a Fish Robot. *Journal of Bionic Engineering* **2009**, *6*, 37–45. doi:https://doi.org/10.1016/S1672-6529(08)60100-6.
3. Shi, L.; Guo, S.; Mao, S.; Yue, C.; Li, M.; Asaka, K. Development of an Amphibious Turtle-Inspired Spherical Mother Robot. *Journal of Bionic Engineering* **2013**, *10*, 446–455. doi:https://doi.org/10.1016/S1672-6529(13)60248-6.
4. Szymak, P.; Przybylski, M. Thrust measurement of biomimetic underwater vehicle with undulating propulsion. *Scientific Journal of Polish Naval Academy* **2018**, *213*, 69–82. doi:10.2478/sjpna-2018-0014.
5. Salazar, R.; Quintana, R.; Abdelkefi, A. Role of Electromechanical Coupling, Locomotion Type and Damping on the Effectiveness of Fish-Like Robot Energy Harvesters. *Energies* **2021**, *14*. doi:10.3390/en14030693.
6. Marcin, M.; Adam, S.; Jerzy, Z.; Marcin, M. Fish-like shaped robot for underwater surveillance and reconnaissance–Hull design and study of drag and noise. *Ocean Engineering* **2020**, *217*, 107889. doi:doi.org/10.1016/J.OCEANENG.2020.107889.
7. Szymak, P.; Malec, M.; Morawski, M. Directions of development of underwater vehicle with undulating propulsion. *Polish Journal of Environmental Studies, Hard Publishing Company* **2010**, *19*, 107–110.
8. Piskur, P.; Gasiorowski, M. Digital Signal Processing for Hydroacoustic System in Biomimetic Underwater Vehicle. *NASE MORE* **2020**, *67*, 14–18. doi:{10.17818/NM/2020/1.3}.
9. Tytell, E.D.; Hsu, C.Y.; Williams, T.L.; Cohen, A.H.; Fauci, L.J. Interactions between internal forces, body stiffness, and fluid environment in a neuromechanical model of lamprey swimming. *Proceedings of the National Academy of Sciences* **2010**, *107*, 19832–19837.
10. Grzadziela, A.; Szymak, P.; Piskur, P. Method for assessing the dynamics and efficiency of diving fins. *ACTA OF BIOENGINEERING AND BIOMECHANICS* **2020**, *22*, 139–150. doi:{10.37190/ABB-01589-2020-06}.
11. Blondeaux, P.; Fornarelli, F.; Guglielmini, L.; Triantafyllou, M.; Verzicco, R. Vortex structures generated by a finite-span oscillating foil. 43rd AIAA aerospace sciences meeting and exhibit, 2005, p. 84. doi:10.2514/6.2005-84.
12. Morawski, M.; Malec, M.; Szymak, P.; Trzmiel, A. Analysis of Parameters of Traveling Wave Impact on the Speed of Biomimetic Underwater Vehicle. Solid State Phenomena. Trans Tech Publ, 2014, Vol. 210, pp. 273–279.

13. Michelin, S.; Llewellyn Smith, S.G. Resonance and propulsion performance of a heaving flexible wing. *Physics of Fluids* **2009**, *21*, 071902.
14. Hozyn, S. An Automated System for Analysing Swim-Fins Efficiency. *NASE MORE* **2020**, *67*, 10–17. doi:{10.17818/NM/2020/3.9}.
15. Szymak, P.; Praczyk, T.; Naus, K.; Szturomski, B.; Malec, M.; Morawski, M. Research on biomimetic underwater vehicles for underwater ISR. Ground/Air Multisensor Interoperability, Integration, and Networking for Persistent ISR VII. International Society for Optics and Photonics, 2016, Vol. 9831, p. 98310L. doi:10.1117/12.2225587.
16. Piskur, P.; Szymak, P.; Jaskólski, K.; Flis, L.; Gąsiorowski, M. Hydroacoustic System in a Biomimetic Underwater Vehicle to Avoid Collision with Vessels with Low-Speed Propellers in a Controlled Environment. *Sensors* **2020**, *20*, 968.
17. Singh, N.; Gupta, A.; Mukherjee, S. A dynamic model for underwater robotic fish with a servo actuated pectoral fin. *SN Applied Sciences* **2019**, *1*, 1–9. doi:10.1007/s42452-019-0679-x.
18. Li, Z.; Xu, W.; Wang, W.; DU, Y.j. Dynamic modeling and experimental research on the linear swimming of a biomimetic cod fish driven by pectoral fin with two degrees of freedom and flexible body. *J Ship Mech* **2017**, *21*, 513–527.
19. Nguyen, T.T.; Lee, B.R.; Vo, T.Q.; others. Dynamic analysis of a robotic fish propelled by flexible folding pectoral fins. *Robotica* **2020**, *38*, 699–718. doi:10.1017/S0263574719000997.
20. Behbahani, S.B.; Tan, X. Bio-inspired flexible joints with passive feathering for robotic fish pectoral fins. *Bioinspiration & biomimetics* **2016**, *11*, 036009. doi:10.1088/1748-3190/11/3/036009.
21. Piskur, P.; Szymak, P.; Flis, L.; Sznajder, J. Analysis of a Fin Drag Force in a Biomimetic Underwater Vehicle. *NAŠE MORE: znanstveni časopis za more i pomorstvo* **2020**, *67*, 192–198. doi:10.17818/NM/2020/3.2.
22. Maertens, A.P.; Triantafyllou, M.S.; Yue, D.K.P. Efficiency of fish propulsion. *Bioinspiration & Biomimetics* **2015**, *10*, 046013. doi:10.1088/1748-3190/10/4/046013.
23. Collins, K.M. The effects of asymmetry on oscillatory propulsion. PhD thesis, University of Bath, 2012.
24. Floryan, D.; Van Buren, T.; Smits, A.J. Efficient cruising for swimming and flying animals is dictated by fluid drag. *Proceedings of the National Academy of Sciences* **2018**, *115*, 8116–8118. doi:10.1073/pnas.1805941115.
25. Liu, G.; Dong, H. Effects of tail geometries on the performance and wake pattern in flapping propulsion. Fluids Engineering Division Summer Meeting. American Society of Mechanical Engineers, 2016, Vol. 50299, p. V01BT30A002. doi:10.1115/FEDSM2016-7691.
26. Engels, T.; Kolomenskiy, D.; Schneider, K.; Sesterhenn, J. Numerical simulation of vortex-induced drag of elastic swimmer models. *Theoretical and Applied Mechanics Letters* **2017**, *7*, 280–285. doi:doi.org/10.1016/j.taml.2017.10.001.
27. Piskur, P.; Szymak, P.; Kitowski, Z.; Flis, L. Influence of fin's material capabilities on the propulsion system of biomimetic underwater vehicle. *Polish Maritime Research* **2020**. doi:10.2478/pomr-2020-0078.
28. Bogdan, S.; Radosław, K. Material Properties of HY 80 Steel after 55 Years of Operation for FEM Applications. *Materials* **2021**, *14*, 4213. doi:10.3390/ma14154213.
29. Piskur, P.; Szymak, P.; Sznajder, J. Identification in a laboratory tunnel to control fluid velocity. In *Advanced, Contemporary Control*; Springer, 2020; pp. 1543–1552.
30. Jurczyk, K.; Piskur, P.; Szymak, P. Parameters identification of the flexible fin kinematics model using vision and Genetic Algorithms. *Polish Maritime Research* **2020**. doi:10.2478/pomr-2020-0025.
31. Buckingham, E. The principle of similitude. *Nature* **1915**, *96*, 396–397.
32. Liu, W.; Xiao, Q.; Cheng, F. A bio-inspired study on tidal energy extraction with flexible flapping wings. *Bioinspiration & biomimetics* **2013**, *8*, 036011.
33. Wu, X.; Zhang, X.; Tian, X.; Li, X.; Lu, W. A review on fluid dynamics of flapping foils. *Ocean Engineering* **2020**, *195*, 106712. doi:10.1016/j.oceaneng.2019.106712.
34. Triantafyllou, G.S.; Triantafyllou, M.S.; Grosenbaugh, M.A. Optimal thrust development in oscillating foils with application to fish propulsion. *Journal of Fluids and Structures* **1993**, *7*, 205–224.
35. Baik, Y.S.; Bernal, L.P. Experimental study of pitching and plunging airfoils at low Reynolds numbers. *Experiments in fluids* **2012**, *53*, 1979–1992.
36. Luo, Y.; Xiao, Q.; Shi, G.; Pan, G.; Chen, D. The effect of variable stiffness of tuna-like fish body and fin on swimming performance. *Bioinspiration & Biomimetics* **2020**, *16*, 016003. doi:10.1088/1748-3190/abb3b6.

37. Bevilaqua, P.; Yam, C. Propulsive Efficiency of Wake Ingestion. *Journal of Propulsion and Power* **2020**, *36*, 517–526. doi:10.2514/1.B37695.
38. Gough, W.T.; Smith, H.J.; Savoca, M.S.; Czapanskiy, M.F.; Fish, F.E.; Potvin, J.; Bierlich, K.; Cade, D.E.; Clemente, J.D.; Kennedy, J.; others. Scaling of oscillatory kinematics and Froude efficiency in baleen whales. *Journal of Experimental Biology* **2021**. doi:10.1242/jeb.237586.
39. Heller, V. 8.04 - Development of Wave Devices from Initial Conception to Commercial Demonstration. In *Comprehensive Renewable Energy*; Sayigh, A., Ed.; Elsevier: Oxford, 2012; pp. 79–110. doi:https://doi.org/10.1016/B978-0-08-087872-0.00804-0.
40. Rodič, M.; Milanovič, M.; Truntič, M. Digital Control of an Interleaving Operated Buck-Boost Synchronous Converter Used in a Low-Cost Testing System for an Automotive Powertrain. *Energies* **2018**, *11*. doi:10.3390/en11092290.
41. De Santis, M.; Agnelli, S.; Patanè, F.; Giannini, O.; Bella, G. Experimental Study for the Assessment of the Measurement Uncertainty Associated with Electric Powertrain Efficiency Using the Back-to-Back Direct Method. *Energies* **2018**, *11*. doi:10.3390/en11123536.
42. Ebrahimi, M.; Abbaspour, M. A comparative numerical study on the performances and vortical patterns of two bioinspired oscillatory mechanisms: undulating and pure heaving. *Applied Bionics and Biomechanics* **2015**, *2015*. doi:https://doi.org/10.1155/2015/325934.
43. Link, O.; Sanhueza, C.; Arriagada, P.; Brevis, W.; Laborde, A.; González, A.; Wilkes, M.; Habit, E. The fish Strouhal number as a criterion for hydraulic fishway design. *Ecological Engineering* **2017**, *103*, 118–126. doi:10.1016/j.ecoleng.2017.03.018.
44. Dabiri, J.O. Optimal vortex formation as a unifying principle in biological propulsion. *Annual review of fluid mechanics* **2009**, *41*, 17–33.
45. Eloy, C. Optimal Strouhal number for swimming animals. *Journal of Fluids and Structures* **2012**, *30*, 205–218. doi:10.1016/j.jfluidstructs.2012.02.008.
46. Riggs, P.; Bowyer, A.; Vincent, J. Advantages of a biomimetic stiffness profile in pitching flexible fin propulsion. *Journal of Bionic Engineering* **2010**, *7*, 113–119. doi:10.1016/S1672-6529(09)60203-1.
47. Taylor, G.K.; Nudds, R.L.; Thomas, A.L. Flying and swimming animals cruise at a Strouhal number tuned for high power efficiency. *Nature* **2003**, *425*, 707–711.
48. Piskur, P.; Szymak, P. Digital Signal Processing for Hydroacoustic Passive Obstacle Detection System in Biomimetic Underwater Vehicle. 2018 INTERNATIONAL CONFERENCE ON APPLIED MATHEMATICS & COMPUTATIONAL SCIENCE (ICAMCS.NET 2018). IEEE Comp Soc, 2018, pp. 110–114. International Conference on Applied Mathematics and Computational Science (ICAMCS.NET), Budapest, HUNGARY, OCT 06-08, 2018, doi:{10.1109/ICAMCS.NET46018.2018.00027}.
49. Cheong, S.; Kim, Y.J.; Chun, J.H.; Kim, J.K.; Huh, S. Integrated Offshore Seismic Survey Using an Unmanned Wave Glider. *Energies* **2021**, *14*. doi:10.3390/en14020297.